ACS APPLIED ENERGY MATERIALS

www.acsaem.org Article

Comparative Study of Ru-Transition Metal Alloys and Oxides as Oxygen Evolution Reaction Electrocatalysts in Alkaline Media

Hongsen Wang and Héctor D. Abruña*

Cite This: *ACS Appl. Energy Mater.* 2022, 5, 11241−11253 Read Online

ACCESS | Metrics & More | Article Recommendations | Supporting Information

ABSTRACT: The oxygen evolution reaction (OER), as the anodic reaction in water electrolyzers, generally exhibits much higher overpotentials than the hydrogen evolution reaction (HER) and thus requires the development of more active, robust, and stable electrocatalysts. In this work, a series of carbon-supported Ru−M alloy nanoparticles (M = Ir, Co, Ni, and Fe), transition metal (TM)-doped RuO_2 nanoparticles such as $Ru_{1-x}Mn_xO_2$, $Ru_{1-x}Co_xO_2$, $Ru_{1-x-y}Mn_xCo_yO_2$, $Ru_{1-x}Fe_xO_2$, $Ru_{1-x}Ni_xO_2$, and $Ru_{1-x}V_xO_2$/C, as well as RuO_2, MnO_2, Co_3O_4, and $Co_{3-x}Mn_xO_4$ nanoparticles have been synthesized with comparable nanoparticle sizes and compared for their OER intrinsic activities in alkaline media. All studied Ru−M alloy nanoparticles exhibited higher OER activity than pure Ru nanoparticles, and among them, $Ru_{1-x}Ir_x$/C (x = 0.3−1) catalysts were found to be the most active. All studied Ru−TM oxide nanoparticles exhibited higher OER activity than the corresponding Ru−TM alloy nanoparticles with 30−50 atom % Co-doped RuO_2/C catalysts being the most active. The OER enhancement on Ru−TM oxides is ascribed to the weaker O adsorption to their surfaces relative to the respective Ru−TM alloys. Small amounts of Mn (≤0.15 atom %)-doped RuO_2 nanoparticles also slightly enhanced the OER kinetics. In contrast to Co and Mn, Ni-, Fe-, and V-doped RuO_2 nanoparticles inhibited the OER. Among Ru−TM oxide nanoparticles, $Ru_{0.7}Co_{0.3}O_2$/C and $Ru_{0.85}Mn_{0.15}O_2$/C represent promising bifunctional catalysts for both the OER and oxygen reduction reaction (ORR).

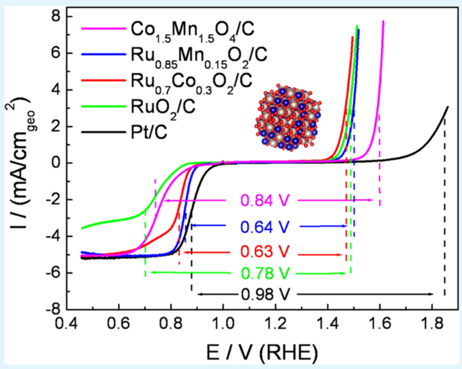

KEYWORDS: *oxygen evolution reaction (OER), Ru alloy nanoparticles, transition metal-doped RuO2, Co−Mn spinel oxides, bifunctional catalysts, synergistic effect, DFT, oxygen adsorption energy*

1. INTRODUCTION

To overcome the limited fossil fuel resources and to mitigate greenhouse gas CO_2 emissions to confront global warming, renewable energy sources such as solar and wind have been explored in recent years. However, these renewable energy sources have a significant disadvantage in that their generation and supply are irregular and vary with time, weather, seasons, and location. To achieve a stable renewable energy supply, energy storage technologies must be developed. Among them, water splitting to generate H_2 and O_2 can play an important role in the development of renewable energy options. Water electrolyzers can convert intermittent renewable energy sources, such as solar and wind, into hydrogen (and oxygen), which can be reconverted into electricity in fuel cells when needed. The oxygen evolution reaction (OER) represents the anodic electrode reaction and is paired with the hydrogen evolution reaction (HER) in water electrolyzers for splitting water. However, the OER involves a four-electron transfer and has much larger overpotentials than the HER, which is one of the outstanding challenges we must confront. For this reason, the OER on different catalysts has been extensively studied over the past decades to elucidate the reaction mechanism in an effort to mitigate the large overpotentials.

The OER takes place at very positive potentials so that in addition to catalyst activity, the stability of OER catalysts is of vital importance. So far, Ru, Ir, and Ru-Ir alloys and their rutile oxides are well known to be very active and stable OER catalysts.[1−4] Titanium substrates coated with RuO_2 + TiO_2, or RuO_2 + IrO_2 + TiO_2, which are called dimensionally stable anodes (DSA), have been used widely in the chlor-alkali industry because of their excellent stability and low overpotentials for the chlorine evolution reaction.[5] They also exhibit high OER activity.[6] Lee et al. studied rutile IrO_2 and RuO_2 nanoparticles for the OER in both acid and alkaline solutions and compared their activity to those of Ru and Ir nanoparticle catalysts. They found that rutile IrO_2 and RuO_2 were highly active for the OER in both acidic and alkaline media and that rutile RuO_2 nanoparticles exhibited slightly higher OER activities than rutile IrO_2 nanoparticles. Ir/C was

Received: June 10, 2022
Accepted: August 30, 2022
Published: September 9, 2022

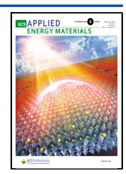

found to be slightly more active for the OER than rutile IrO_2 nanoparticles but less stable. In contrast, Ru/C catalysts were less active and degraded much faster than Ir/C and rutile RuO_2.[2] Reier et al. compared the OER activity and stability of bulk and nanoparticle Ru, Ir, and Pt catalysts in acidic media and found that bulk Ir and nanoparticle Ir catalysts exhibited comparably high OER activity and durability. However, the performance of nanoparticle Ru was very poor, while bulk Ru exhibited a very high OER activity.[7] Cherevko et al. studied the activity and stability of well-defined Ru, RuO_2, Ir, and IrO_2 thin film electrodes in acidic and alkaline electrolytes, and found that OER activity decreased as Ru > Ir ≈ RuO_2 > IrO_2 in both electrolytes, while dissolution increased as $IrO_2 \ll RuO_2 < Ir \ll Ru$. Moreover, the dissolution rate of these metals in both solutions was 2−3 orders of magnitude higher when compared to their respective oxides, and their dissolution was generally higher in alkaline solutions.[3] Danilovic et al. reported that the order of OER activity of monometallic oxides in acid media was Os ≫ Ru > Ir > Pt > Au, but the stability order was the reverse.[8]

Transition-metal-doped Ru, Ir, RuO_2, and IrO_2 have also been studied by several groups. Halck et al. reported that Co- and Ni-modified ruthenia were more active than unmodified ruthenia for the OER in acidic media and claimed that they were beyond the volcano limitations (i.e., their activity appeared significantly above the peak of the conventional volcano plot).[9] Forgie et al. studied bimetallic Ru−M alloys (M = Pd, Ir, Cu, Co, Re, Cr, Ni) for the OER in acidic media and found that Ru−Co, Ru−Ir, and Ru−Cu exhibited improved OER activity.[10] Mixtures of manganese oxides and ruthenium oxide have also been studied as bifunctional catalysts for the oxygen reduction reaction (ORR) and OER.[11] Browne et al. reported that mixed Mn/Ru oxides with 10% Mn and an annealing temperature of 350 °C exhibited the highest OER activity and even had a lower overpotential than RuO_2 and IrO_2.[12]

Kötz et al. studied the OER on a series of sputtered Ru−Ir alloys with different Ir content in 1 M H_2SO_4 and found that the stability increased with increasing Ir content while the OER activity decreased.[4] The OER on sputtered $Ru_xIr_{1-x}O_2$ was also studied by the same authors. They reported that small additions of IrO_2 to RuO_2 reduced the galvanostatic corrosion rate significantly. An optimal trade-off between stability and activity was found for $0.5 < x < 0.8$.[4]

Yeo et al. reported that the electrocatalytic activity of ruthenium oxide can be improved and stabilized in an acid electrolyte by alloying with iridium and tantalum, probably because the ruthenium cations in these mixed oxides can exist in the III−IV state and remain in such mixed valences over long periods of time. Ternary Ru and Ir oxides such as Sn−Ir−Ru oxides and Ta−Ir−Ru oxides have also been reported to increase activity and stability in acidic media.[13,14] Kim et al. reported that a pyrochlore yttrium ruthenate ($Y_2Ru_2O_{7-\delta}$) exhibited significantly enhanced activity for the OER in 0.1 M perchloric acid when compared to RuO_2.[15]

In alkaline media, transition metal (TM) oxides can be more stable than in acidic media, and thus, Ni-, Co-, Fe-, and Mn-based single metal oxides, binary metal oxides, ternary metal oxides, and perovskites have been studied/explored as potential OER catalysts.[5,16−21] However, their OER activity and stability are still inferior to those of RuO_2 and IrO_2 catalysts.

Nickel is one of the most promising transition metal OER catalysts in alkaline media, and its surface is normally covered with a Ni (oxy)hydroxide layer at anodic potentials in alkaline media. $NiFe(OH)_2$ has been reported to exhibit an enhanced OER activity when compared to $Ni(OH)_2$.[22−28] However, these types of catalysts are not active for the oxygen reduction reaction (ORR), and thus cannot be used as bifunctional catalysts for both OER and ORR.

Among perovskites, $SrCoO_3$ and $LaNiO_3$ were identified as the best oxygen evolution catalysts.[29] Suntivich et al. reported that $Ba_{0.5}Sr_{0.5}Co_{0.8}Fe_{0.2}O_{3-\delta}$ (BSCF) exhibited an order of magnitude higher OER activity than that of the state-of-the-art iridium oxide catalyst in alkaline media.[30]

According to the literature, the catalytic activity could vary significantly from bulk materials, films, to nanoparticles, from metal oxides formed by thermal decomposition to electrochemically formed metal oxides, from metals to their oxides, and from acidic media to alkaline media. The direct comparison of the intrinsic OER activity of these different catalysts is challenging since the surface area might be significantly different.

While in alkaline media, non-noble metal alloys and metal oxides can exhibit some OER activity and stability, their long-term durability remains a big challenge. Combining non-noble metals with noble metals can enhance the activity and stability of OER catalysts, though the cost increases. There is an optimal trade-off between/among cost, activity, and stability. Ru and RuO_2 have been extensively studied in acidic media as OER catalysts, but their study in alkaline media has been limited. In alkaline media, due to the higher stability of transition metals relative to acidic media, doping Ru or RuO_2 with transition metals can provide options to further enhance the OER activity and reduce the amount of noble metal employed without significantly compromising stability.

As practical catalysts, nanoparticle catalysts are usually employed to increase surface area and thus reduce the amount/weight of catalyst employed. However, Ru nanoparticles exhibited much lower OER activity than bulk Ru. To enhance the OER activity of Ru nanoparticles, in this work, we doped Ru nanoparticles with different levels of Ir and compared their OER activity in alkaline media with Ru nanoparticles doped with Co, Ni, and Fe.[31] To minimize particle size effects, the nanoparticles were synthesized to have a similar particle size and thus had comparable surface areas. Furthermore, we synthesized RuO_2 nanoparticles doped with Co, Fe, Ni, Mn, and V and compared their OER activity and stability with the Ru−M (M = Co, Ni, Fe, and Ir) alloy nanoparticles. We found that RuO_2 and doped RuO_2 nanoparticles are much more active and stable than their respective Ru and Ru−M alloy nanoparticles and $Ru_{1-x}Co_xO_2$/C (x = 0.3−0.5) exhibited the highest OER activity among all studied electrocatalysts. Finally, we propose that Mn- and Co-doped RuO_2 nanoparticles could be used as effective bifunctional catalysts for both OER and ORR, and $Co_{1.5}Mn_{1.5}O_4$/C is also a promising nonprecious-metal bifunctional catalyst.

2. EXPERIMENTAL SECTION

2.1. Synthesis and Characterization of Carbon-Supported Nanoparticle Catalysts. A series of Vulcan XC-72R-supported Ru alloy nanoparticle catalysts—$Ru_{1-x}Ir_x$/C ($0.1 \le x \le 0.9$), and $Ru_{1-x}Co_x$/C, $Ru_{1-x}Ni_x$/C, and $Ru_{1-x}Fe_x$/C ($0.05 \le x \le 0.5$)—with a metal loading of 11 wt %, as well as Ir/C, Ru/C, and Pt/C

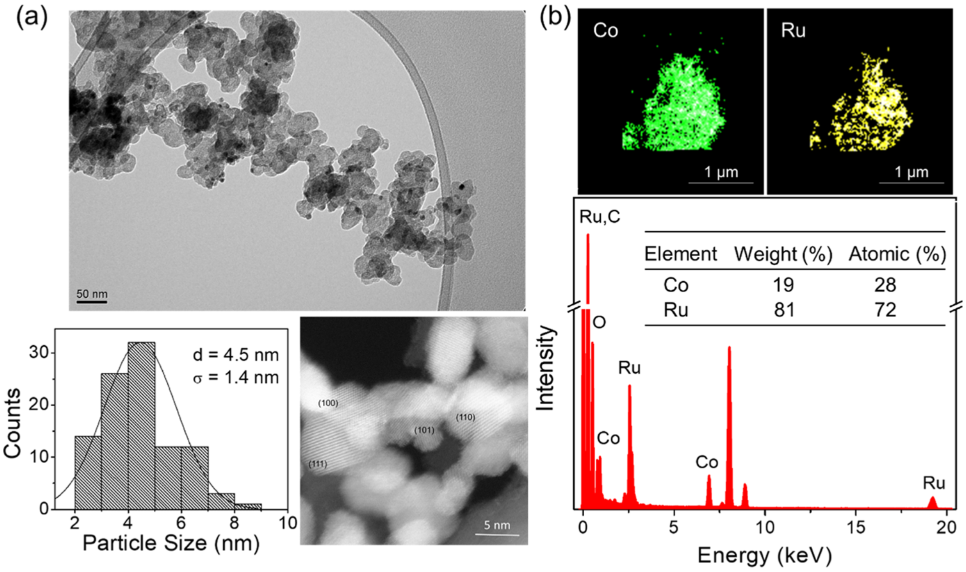

Figure 1. (a) TEM images and nanoparticle distribution histogram of $Ru_{0.7}Co_{0.3}O_2/C$. (b) EDX maps of Ru and Co for $Ru_{0.7}Co_{0.3}O_2/C$ and its elemental composition.

nanoparticles with a metal loading of 20 wt % were synthesized by a wet-impregnation method with chloride or nitrate precursors and subsequent thermal decomposition of the precursor salts, followed by reduction with forming gas. The synthesis details have been described in a previous paper.[31]

A series of Vulcan XC-72R-supported Ru-transition metal binary and ternary oxide nanoparticle catalysts—$Ru_{1-x}Mn_xO_2/C$, $Ru_{1-x}Co_xO_2/C$, $Ru_{1-x}Ni_xO_2/C$, $Ru_{1-x}Fe_xO_2/C$, $Ru_{1-x}V_xO_2/C$ ($0.05 \le x \le 0.9$), $Ru_{1-x-y}Mn_xCo_yO_2/C$, as well as RuO_2/C, and $Co_{3-x}Mn_xO_4/C$ nanoparticles with a metal loading of 11 wt % were also synthesized via a wet-impregnation method with nitrate precursors, subsequent thermal decomposition of precursor salts, and then annealing in air for 2 h at high temperatures, as described in a previous paper.[32]

The catalysts were characterized by powder X-ray diffraction (XRD) in a Rigaku Ultima VI diffractometer with a Cu Kα source (λ = 0.15418 nm). Data were collected at a scan rate of 5°/min and with an increment step of 0.02°.

Bright-field transmission electron microscopy (TEM) was performed using an FEI Tecnai 12 BioTwin TEM operated at 120 kV, while dark-field TEM was performed on a Nion 100 UltraSTEM.

An LEO 1550 instrument, in which a field emission scanning electron microscope (FESEM) was equipped with an energy-dispersive X-ray (EDX) spectrometer, or an FEI Tecnai F20 S/TEM were used to perform EDX spectroscopy. The surface composition of samples was analyzed with SSX-100 X-ray photoelectron spectroscopy (XPS) at a high sensitivity scan.

A TA Instruments Q500 thermogravimetric analyzer (TGA) was used to confirm catalyst loadings.

2.2. Thin Film Electrode Preparation. First, a catalyst ink was prepared by mixing the catalyst powder containing 0.8 mg metal, 3.2 mL of Millipore water, 0.8 mL of isopropanol, and 40 μL of Nafion solution (5 wt %, Fuel Cell Store), and subsequently sonicating for 15 min. A glassy carbon (GC) rotating disk electrode (RDE) with a diameter of 6 mm was polished with 1 μm diamond paste (Buehler) and then rinsed with acetone and Millipore water, respectively. Afterward, 20 μL of catalyst ink was pipetted onto the GC electrode and subsequently dried in air. To enhance the uniformity of the catalyst film, the GC electrode was dipped into 0.1 M KOH for 10 min, leading to its surface becoming more hydrophilic. A homogeneously dispersed thin film of catalyst was formed on the GC electrode with a catalyst loading of 14 $\mu g_{metal}/cm^2$.

2.3. Electrochemical Measurements. Electrochemical experiments were carried out with a WaveDriver 20 Bipotentiostat/Galvanostat and AfterMath software (Pine Research Instrumentation). A three-electrode electrochemical cell made of Teflon was used for alkaline media to avoid contamination from dissolved glass. An AFMSRCE Rotator (Pine Research Instrumentation) was used for the oxygen evolution measurements at rotation rates of 400 or 1600 rpm. A homemade Ag/AgCl (1 M NaCl) electrode was used as the reference electrode, and all potentials are quoted relative to a reversible hydrogen electrode (RHE) with an electrolyte of 0.1 M KOH. A Pt wire was used as the counter electrode. The supporting electrolyte was prepared using Millipore water (18.2 MΩ·cm) and potassium hydroxide (99.99%, Sigma-Aldrich). Before measurements, all solutions were deaerated with high-purity Ar (Airgas). All experiments were carried out at room temperature (20 ± 1 °C).

To compare mass activity (MA), the OER currents were normalized to the mass of metals or the mass of noble metals.

The electrochemical surface areas (ECSA) of bulk Pt, Ir, and Ru and nanoparticle Pt/C, Ir/C, Ru/C, $Ru_{1-x}Co_x/C$, $Ru_{1-x}Ni_x/C$, $Ru_{1-x}Fe_x/C$, and $Ru_{1-x}Ir_x/C$ catalysts were estimated by H upd.[31] In contrast, the ECSA of RuO_2/C were estimated from the mean particle size, assuming the particles had a spherical shape. The ECSA of the transition metal-doped RuO_2/C catalysts were determined by comparing their double layer capacitances to that of RuO_2/C.[32] It should be noted that the contribution of pure carbon to the whole double layer capacitances was very small and could be neglected (see Figure S1). The ECSA of Co_3O_4/C, MnO_2/C, and $Co_{3-x}MnO_4/C$ was also estimated from their mean particle size. The OER currents were normalized to the ECSA to compare their specific activity (SA).

3. RESULTS

3.1. Nanoparticle Characterization. X-ray diffraction data of a series of carbon-supported Ru, Ir, Pt, $Ru_{1-x}Ir_x$, $Ru_{1-x}Co_x$, $Ru_{1-x}Ni_x$, and $Ru_{1-x}Fe_x$ nanoparticles are presented in Figures S2 and S3. All studied Ru alloy nanoparticles with a low content of the second metal ($0 \le x \le 0.5$) exhibited the same hexagonal close-packed (hcp) structure as Ru nanoparticles. As the Ir content increased up to 70 and 90 atom %, the Ru−Ir alloys changed into a face-centered cubic (fcc) structure. Co and Fe have a higher solubility in Ru, so Co and Fe can fully alloy with Ru even at the high Co and Fe content of 50 atom %. In contrast, Ni is less soluble in Ru than Co and Fe, so Ru and Ni could not fully form alloys, and NiO diffraction peaks were evident when the nominal Ni content

https://doi.org/10.1021/acsaem.2c01545
ACS Appl. Energy Mater. 2022, 5, 11241−11253

reached 50 atom %.[31] According to Vegard's law, the lattice parameters of $Ru_{1-x}Ir_x$/C should increase with increasing Ir content, while the lattice parameters of $Ru_{1-x}Co_x$/C, $Ru_{1-x}Ni_x$/C, and $Ru_{1-x}Fe_x$/C should decrease with increasing Co, Ni, and Fe content. The lattice parameters determined from XRD were in good agreement with those calculated from Vegard's law, suggesting that Ru and the other transition metals are fully and uniformly alloyed in all samples. The mean particle sizes were estimated from Rietveld analysis to be about 3 nm. Representative TEM images of Ru alloys are presented in Figures S4–S7. The nanoparticles are quite well distributed on Vulcan, and the mean nanoparticle sizes were also estimated from TEM and were in good agreement with those estimated from XRD (Table S1).

The X-ray diffraction data of a series of carbon-supported transition metal (TM)-doped RuO_2 nanoparticles are presented in Figures S8 and S9. All studied Ru–TM oxide nanoparticle catalysts exhibited the same tetragonal (rutile) structure as RuO_2/C. The addition of Co and Mn into the RuO_2 lattices resulted in a decrease in the lattice parameters—*a*, *b*, and *c*. When the content of Mn and Co was too high, two separate phases (phase segregation) were observed. At an Mn content of 0.8, two rutile phases could be ascribed to Mn-doped RuO_2 and Ru-doped MnO_2, respectively. At a Co content of over 0.3, besides a rutile phase, a spinel structure also appeared. So was the case for the ternary oxide—$Ru_{0.1}Mn_{0.6}Co_{0.3}O_2$/C. Ni-, Fe-, and V-doped RuO_2/C catalysts with a content of 0.3 exhibited comparable parameters to RuO_2/C (Figure S9a). $Co_{3-x}Mn_xO_4$/C nanoparticles exhibited a cubic spinel structure, and their lattices shrank with an increase in Co content (Figure S9b). The nanoparticle sizes of all studied catalysts, estimated from XRD data using Rietveld analysis, are listed in Table S2. TEM images suggested that the oxide nanoparticles were also quite well dispersed on the Vulcan support, as shown in Figures 1a and S10. The nanoparticle size of all transition metal-doped RuO_2/C catalysts was about 5 nm, and the nanoparticle size of spinel $Co_{3-x}Mn_xO_4$/C catalysts was about 3 nm.

As examples, the EDX spectra and elemental composition of $Ru_{0.7}Co_{0.3}O_2$/C were determined with scanning transmission electron microscopy (STEM)-EDX, and are shown in Figure 1b, with values consistent with the nominal composition employed in the synthesis. The surface elemental composition of $Ru_{0.7}Co_{0.3}O_2$/C, determined via XPS (Figure S11 and Table S4), is also in good agreement with the nominal composition, suggesting that Co is quite well distributed in the nanoparticles. The metal loadings of catalysts on Vulcan were verified with TGA and were in good agreement with the nominal loadings (11 wt %) (see Figure S12).

The catalysts were also characterized via cyclic voltammetry in 0.1 M KOH, as shown in Figures S13 and S14. Transition metal doping can apparently affect the cyclic voltammetric profiles of Ru/C and RuO_2/C. For example, Mn- and Co-doped RuO_2/C exhibited Mn and Co redox peaks at potentials between 0.2 and 1.0 V (vs RHE), and their redox peak intensity increased with increasing Mn and Co content. Low levels of transition metal doping into Ru significantly enhanced H adsorption/desorption reversibility/kinetics. Further increasing the content of transition metals reduced H adsorption/desorption charge, suggesting that the surface Ru content decreased.

3.2. Oxygen Evolution Reaction (OER) on Ru Alloy Catalysts. *3.2.1. Comparison of OER Activity on Bulk Ru, Ir, and Pt and Nanoparticle Ru/C, Ir/C, Pt/C, and RuO_2/C Catalysts.* Linear sweep voltammetric (LSV) profiles of bulk Ru, Ir, and Pt electrodes and Ru/C, Ir/C, Pt/C, and RuO_2/C nanoparticle catalysts for the OER in 0.1 M KOH at a rotating rate of 400 rpm and a scan rate of 5 mV/s are presented in Figure 2. The third positive-going-scan LSV profiles are shown for comparison. Figure 2a compares the specific activity (SA) for the OER on bulk electrodes and nanoparticle catalysts, while Figure 2b compares the mass activity (MA) for the OER on nanoparticle catalysts. The bulk Ru electrode exhibited a very high specific activity for the OER, while the Ru/C nanoparticle catalyst was much less active than the bulk Ru in alkaline media. Similarly, a bulk Pt electrode was also more active than Pt/C for the OER in 0.1 M KOH. This is similar to the case in acidic media.[7] In contrast, the Ir/C nanoparticle catalyst exhibited a higher SA for the OER than the bulk Ir electrode and was significantly more active than the Ru/C nanoparticle catalyst. Thus, it appears that the nanoparticle size effect for the OER on Ir/C nanoparticles is different from that on Ru/C and Pt/C. In general, the SA of Pt or Pd for electrocatalytic reactions such as the ORR, hydrogen oxidation/evolution reactions, CO, and fuel oxidation reactions decreases with decreasing nanoparticle size due to an increase in the adsorption energy.[33−38] In contrast, the enhanced OER activity for Ir nanoparticles could be due to the exposure of different facets[39] or to different coverages of surface oxide species formed.[40] Similarly, we have previously found that small Rh nanoparticles exhibited an enhanced activity for the hydrogen oxidation/evolution reactions in alkaline media. This is likely due to the weaker adsorbed

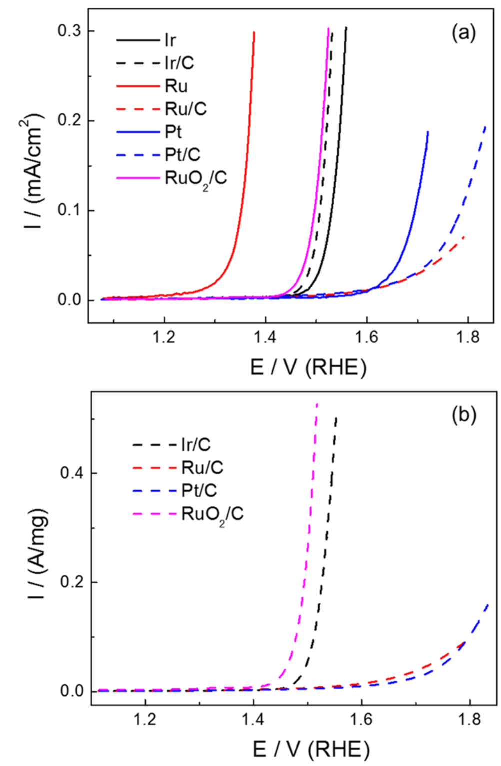

Figure 2. LSV profiles of Ru/C, Ir/C, and Pt/C catalysts, and Ru, Ir, and Pt bulk electrodes for the OER in 0.1 M KOH. Scan rate: 5 mV/s. (a) Current is normalized to the ECSA; (b) current is normalized to the mass of metals.

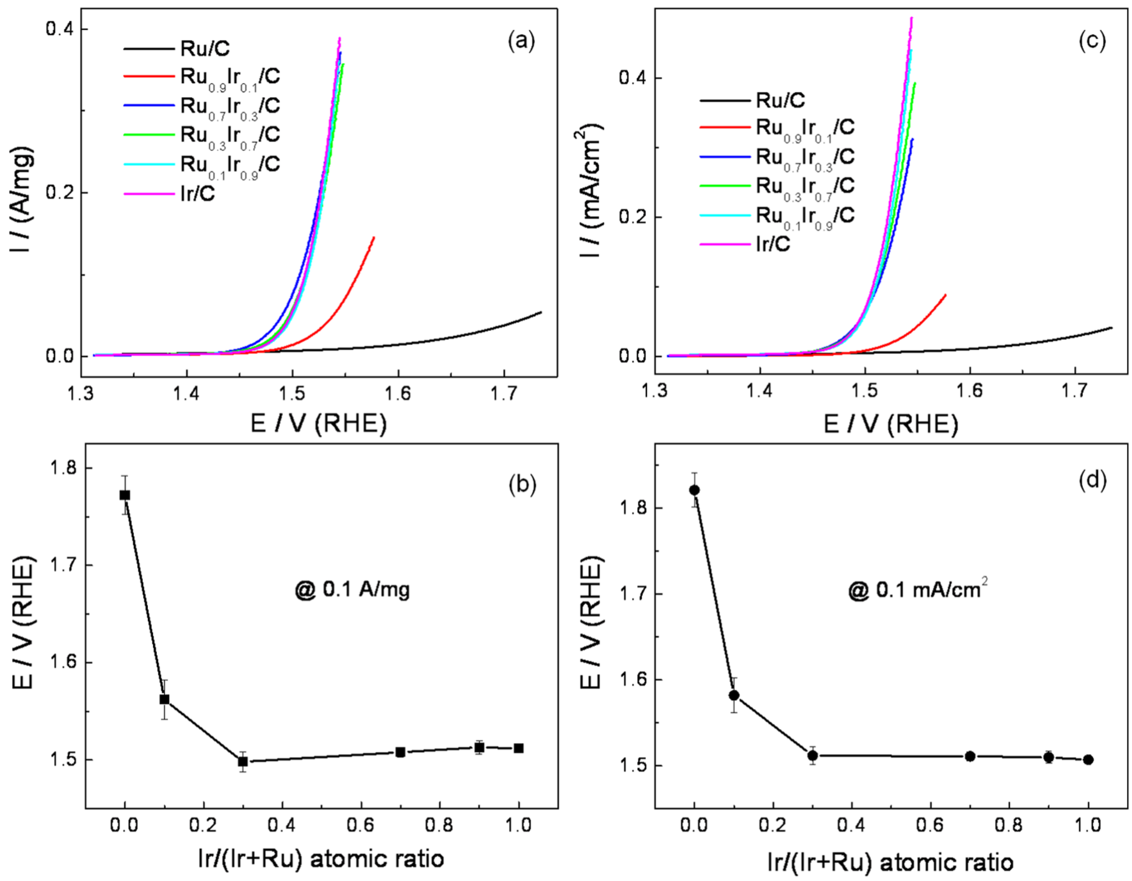

Figure 3. (a) Metal mass-normalized LSV profiles of $Ru_{1-x}Ir_x/C$, Ru/C, and Ir/C catalysts for the OER in 0.1 M KOH. Scan rate: 5 mV/s. (b) OER potential at 0.1 A/mg plotted vs Ir content. (c) ECSA-normalized LSV profiles of $Ru_{1-x}Ir_x/C$, Ru/C, and Ir/C catalysts for the OER in 0.1 M KOH. (d) OER potential at 0.1 mA/cm^2 plotted vs Ir content.

hydrogen formed on Rh(111) facets of small nanoparticles.[41] RuO_2/C exhibited a much higher specific activity for the OER and much higher stability than Ru/C (Figures S15a and S16a). The SA decreased in the following order for the bulk electrodes: Ru > Ir > Pt, while for the nanoparticle catalysts, the order was: RuO_2/C > Ir/C > Pt/C > Ru/C. The MA for the OER on nanoparticle catalysts (Figure 2b) also decreased in the same order as the SA, and RuO_2/C was even more active than Ir/C in terms of MA. It should be noted that although the bulk Ru electrode is very active for the OER in 0.1 M KOH, it readily dissolved to form soluble Ru oxides, and the solution quickly became yellow during the OER.[42]

3.2.2. OER on $Ru_{1-x}Ir_x/C$ Catalysts. To enhance the OER activity and stability of Ru nanoparticles, Ir was alloyed with Ru nanoparticles. LSV profiles of $Ru_{1-x}Ir_x/C$ catalysts for the OER in 0.1 M KOH at a scan rate of 5 mV/s are presented in Figure 3a. For comparison, LSV profiles of Ru/C and Ir/C are also shown. The OER potential at 0.1 A/mg is plotted vs Ir content in Figure 3b. $Ru_{1-x}Ir_x/C$ alloy nanoparticle catalysts show a significantly enhanced OER activity in terms of MA when compared to Ru/C. $Ru_{0.7}Ir_{0.3}/C$ exhibited the highest MA for the OER among all studied $Ru_{1-x}Ir_x/C$ alloy nanoparticle catalysts, even slightly more active than Ir/C (Figure 3a,b). When the OER current was normalized to the ECSA, $Ru_{0.7}Ir_{0.3}/C$, $Ru_{0.3}Ir_{0.7}/C$, $Ru_{0.1}Ir_{0.9}/C$, and Ir/C exhibited a comparable SA for the OER (Figure 3c,d). The Tafel slope decreased from 370 mV for Ru/C to 55 mV for $Ru_{0.7}Ir_{0.3}/C$ (Figure S17). In addition, the stability of $Ru_{1-x}Ir_x/C$ catalysts increased as the Ir content increased (Figure S15).

3.2.3. OER on $Ru_{1-x}Co_x/C$, $Ru_{1-x}Ni_x/C$, and $Ru_{1-x}Fe_x/C$ Catalysts. We have previously studied the OER activity of Ru alloy nanoparticle catalysts with 3d TMs such as Co, Ni, and Fe.[31] We found that Ru−TM (TM = Co, Ni, or Fe) with a TM content of ∼30 atom % exhibited the highest OER activity in 0.1 M KOH, and Ru−Co alloy nanoparticles were more active than Ru−Ni and Ru−Fe alloy nanoparticles. The MA of the OER decreased in the following order: Ir/C ≈ $Ru_{0.7}Ir_{0.3}/C$ > $Ru_{0.7}Co_{0.3}/C$ > $Ru_{0.7}Ni_{0.3}/C$ > $Ru_{0.7}Fe_{0.3}/C$ > Ru/C (Figure S18). The SA also exhibited a similar trend to the MA. In Figure 4, the LSV profiles of $Ru_{0.7}Co_{0.3}/C$, $Ru_{0.7}Ni_{0.3}/C$, and $Ru_{0.7}Fe_{0.3}/C$ catalysts for the OER are further compared with $Ru_{0.7}Ir_{0.3}/C$, Ir/C, and Ru/C, when normalized to the total mass of noble metals. $Ru_{0.7}Co_{0.3}/C$ exhibited a comparable activity to $Ru_{1-x}Ir_x/C$ (x = 0.3−1) in terms of the mass of noble metals. Although these alloy nanoparticle catalysts were much more active than pure Ru nanoparticles, the OER current gradually decreased with potential cycling (Figure S15), suggesting that these carbon-supported Ru−TM alloy nanoparticle catalysts are unstable. This could be caused by both carbon corrosion as well as metal dissolution. To increase the stability of catalysts, more stable supports such as metal oxides need to be developed to replace carbon. In addition, we found that these Ru−TM alloy catalysts were still less active than RuO_2/C (Figure 4d).

3.3. OER on Metal Oxide Catalysts. *3.3.1. Comparison of OER Activity between Ru−TM Alloys and Ru−TM Oxides.* Metal mass-normalized cyclic voltammograms for the OER on RuO_2/C, $Ru_{0.7}Co_{0.3}O_2/C$, $Ru_{0.7}Ni_{0.3}O_2/C$, and $Ru_{0.7}Fe_{0.3}O_2/C$

https://doi.org/10.1021/acsaem.2c01545
ACS Appl. Energy Mater. 2022, 5, 11241−11253

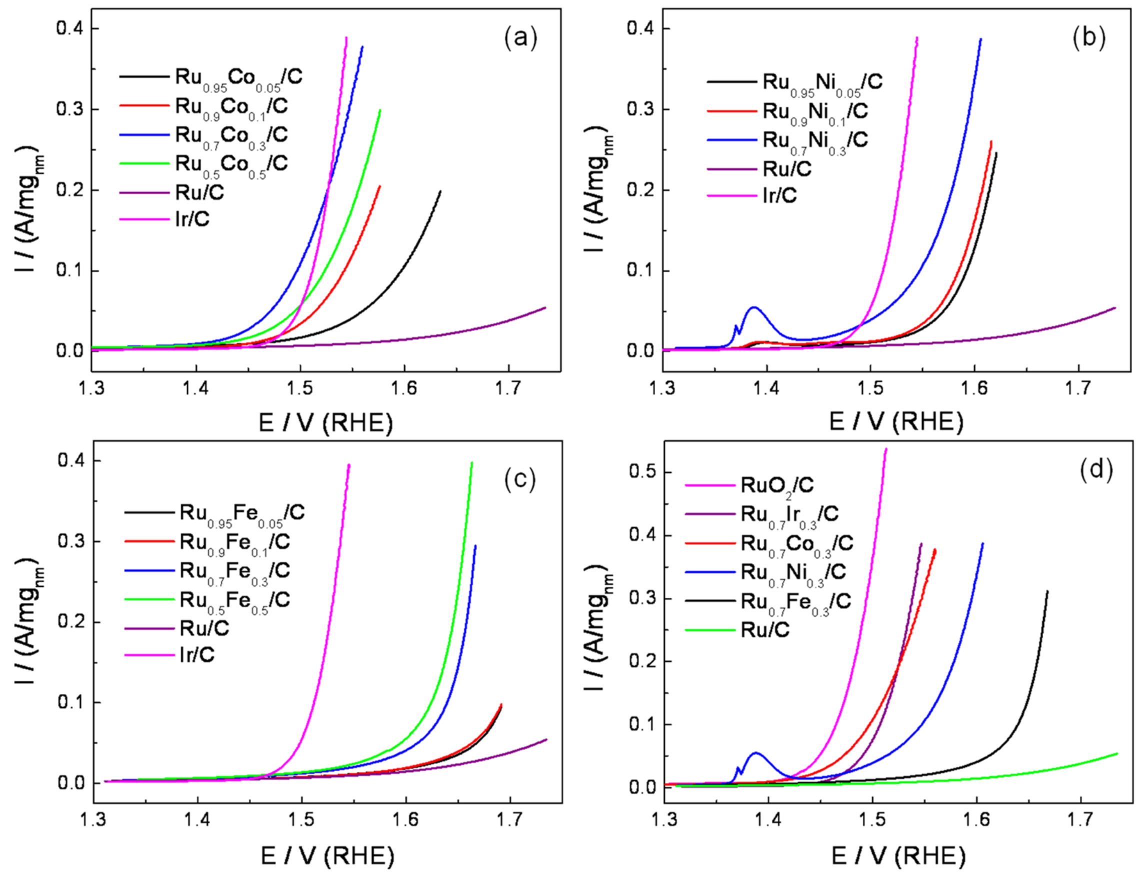

Figure 4. Noble metal (nm) mass-normalized LSV profiles of (a) $Ru_{1-x}Co_x/C$, (b) $Ru_{1-x}Ni_x/C$, and (c) $Ru_{1-x}Fe_x/C$ catalysts for the OER in 0.1 M KOH. Scan rate: 5 mV/s. (d) Comparison of noble metal (nm) mass-normalized LSV profiles of $Ru_{0.7}Ir_{0.3}/C$, $Ru_{0.7}Co_{0.3}/C$, $Ru_{0.7}Ni_{0.3}/C$, $Ru_{0.7}Fe_{0.3}/$, Ru/C, and RuO_2/C for the OER in 0.1 M KOH. The compositions of catalysts are indicated in the figures.

in 0.1 M KOH are compared with Ru/C, $Ru_{0.7}Co_{0.3}/C$, $Ru_{0.7}Ni_{0.3}/C$, and $Ru_{0.7}Fe_{0.3}/C$ in Figure 5. Similar to the case

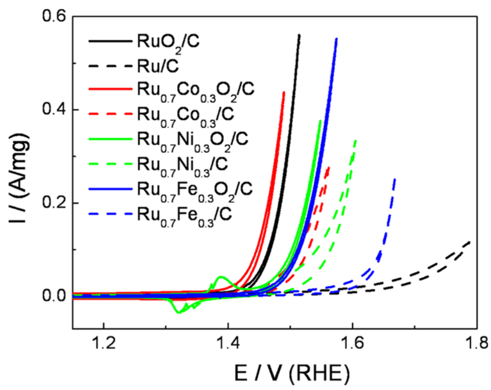

Figure 5. Total metal mass-normalized cyclic voltammograms of RuO_2/C, $Ru_{0.7}Co_{0.3}O_2/C$, $Ru_{0.7}Ni_{0.3}O_2/C$, and $Ru_{0.7}Fe_{0.3}O_2/C$ (solid lines) for the OER in 0.1 M KOH, compared with their respective alloy nanoparticles (dash lines). Scan rate: 5 mV/s.

of RuO_2/C and Ru/C (Figure 4d), all studied Ru−TM oxide nanoparticle catalysts were also much more active than their respective alloy nanoparticle catalysts when normalized to the total metal mass. For the pure Ru and Ru−TM alloy nanoparticle catalysts, their surfaces were already oxidized to form RuO_2 and $Ru_{1-x}TM_xO_2$ oxides around 1.4 V (vs RHE) in the first positive scan (Figure S15).[43] According to the double layer charges (Figure S1) and oxidation/reduction peaks for Ni^{2+}/Ni^{3+} between 1.3 and 1.4 V (Figure 5),[44] the Ru−TM oxide nanoparticle catalysts and Ru−TM alloy nanoparticle catalysts had comparable surface areas. However, all Ru−TM oxide nanoparticle catalysts were much more active than all respective Ru−TM alloy nanoparticle catalysts, suggesting that besides the composition of surface species, the crystal structure and composition of the nanoparticles and thus their resulting electronic effects also play an important role in the OER in alkaline media. Therefore, we next focus on the more stable and more active TM-doped RuO_2/C catalysts.

3.3.2. OER on $Ru_{1-x}Co_xO_2/C$ Catalysts. The effect of Co content in Co-doped RuO_2/C on the OER activity is presented in Figure 6. Ir/C, RuO_2/C, and Co_3O_4/C are also shown for comparison. Total metal mass-normalized LSV profiles (Figure 6a) show that RuO_2/C had a 30 mV lower overpotential than Ir/C, while they exhibited similar Tafel slopes, i.e., 51 mV for RuO_2/C vs 45 mV for Ir/C (Figure S19). Co_3O_4/C exhibited an overpotential that was 120 mV higher than that for RuO_2/C but a similar Tafel slope to RuO_2/C (Figure S19). Low levels (5−20 atom %) of Co doping into RuO_2/C did not significantly change the OER activity in terms of MA or SA. When the atomic percentage of Co increased to 0.3−0.5, both the MA and SA for the OER significantly increased. However, further increases in the Co content to 0.8 caused a decrease in the overall OER activity. Halck et al. also found that in acidic media, Co-doped RuO_2 could significantly enhance the OER activity.[9] When the currents are normalized to the mass of the noble metal, the Co-

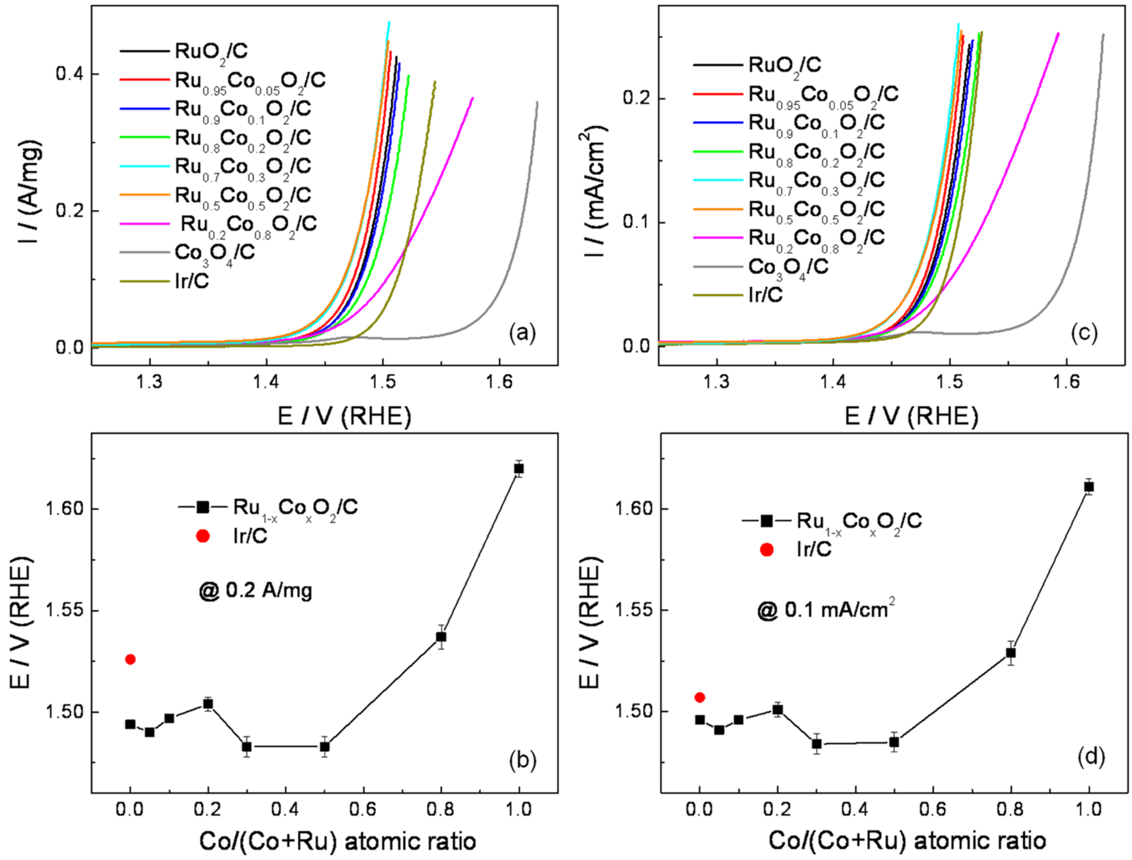

Figure 6. (a) Total metal mass-normalized LSV profiles of RuO_2/C, Ir/C, Co_3O_4/C, and $Ru_{1-x}Co_xO_2$/C catalysts for the OER in 0.1 M KOH. Scan rate: 5 mV/s. (b) OER potential at 0.2 A/mg plotted vs Co content. (c) ECSA-normalized LSV profiles of RuO_2/C, Ir/C, Co_3O_4/C, and $Ru_{1-x}Co_xO_2$/C catalysts for the OER in 0.1 M KOH. (d) OER potential at 0.1 mA/cm^2 plotted vs Co content.

doped RuO_2/C with a Co content of 50 atom % exhibited the highest activity for the OER (Figure S20). Although $Ru_{1-x}Co_xO_2$ (x = 0.3−0.5) nanoparticles exhibited an enhanced activity for the OER, they were less stable than RuO_2. The stability of $Ru_{1-x}Co_xO_2$ catalysts decreased with increasing Co content (Figure S16).

3.3.3. OER on $Ru_{1-x}Mn_xO_2$/C Catalysts. Total metal mass-normalized LSV profiles for the OER on $Ru_{1-x}Mn_xO_2$/C catalysts are compared with RuO_2/C and MnO_2/C in Figure 7a, while the ECSA-normalized LSV profiles are presented in Figure 7c. The OER potentials at 0.2 A/mg and 0.1 mA/cm^2 are plotted vs Mn content in Figure 7b,d, respectively. The MnO_2/C catalyst exhibited an overpotential of 150 mV higher than RuO_2/C for the OER and over 30 mV higher overpotential than Co_3O_4/C. Small amounts of Mn (atomic ratio of Mn/(Ru + Mn) ≤15%) doping into RuO_2/C slightly enhanced the OER activity. The Tafel slope of $Ru_{0.9}Mn_{0.1}O_2$/C was ca. 55 mV, which is smaller than the value of 78 mV for MnO_2/C, but comparable to the value of 51 mV for RuO_2/C (Figure S19). Further increasing the Mn content resulted in a lower OER activity than RuO_2/C. It should be pointed out that although $Ru_{0.2}Mn_{0.8}O_2$/C was not single-phase, it still exhibited quite high OER activity and was even more active than $Ru_{1-x}Mn_xO_2$/C ($0.2 \leq x \leq 0.5$) in terms of MA (Figure 7b). When the OER current is normalized to the mass of the noble metal, the $Ru_{0.2}Mn_{0.8}O_2$/C is superior to other studied Mn-doped RuO_2/C catalysts (Figure S21). Browne et al. also reported that thermally prepared mixed Mn and Ru oxide films with a low Mn content of 10−25 atom %, supported on Ti, exhibited enhanced OER activity relative to a pure RuO_2 film.[12]

3.3.4. OER on $Co_{3-x}Mn_xO_4$/C Catalysts. Prior to studying the ternary oxide $Ru_{1-x-y}Mn_xCo_yO_2$/C catalysts for the OER in alkaline media, we first investigated the OER activity of the binary oxide $Co_{3-x}Mn_xO_4$/C catalysts. The OER activities of Co_3O_4/C, MnO_2/C, and $Co_{3-x}Mn_xO_4$/C are compared in Figure 8a,b. In a previous paper, we found that MnO_2 was more active than Co_3O_4 for the ORR in alkaline media.[32] In this work, Co_3O_4/C was found to be more active than MnO_2/C for the OER in alkaline media. Spinel structure $Co_{3-x}Mn_xO_4$/C nanoparticle catalysts significantly enhanced the OER activity when compared to Co_3O_4/C and MnO_2/C. This suggests that a synergist effect is also present for the OER on $Co_{3-x}Mn_xO_4$/C catalysts, similar to that for the ORR.[32] Among them, $Co_2Mn_1O_4$/C and $Co_{1.5}Mn_{1.5}O_4$/C exhibited the highest OER activity. The Tafel slope for the OER on $Co_2Mn_1O_4$/C and $Co_{1.5}Mn_{1.5}O_4$/C was 55−56 mV, comparable to the value of 51 mV for RuO_2/C (Figure S19). In a previous paper,[32] $Co_1Mn_2O_4$/C and $Co_{1.5}Mn_{1.5}O_4$/C were found to exhibit the highest ORR catalytic activity in alkaline media. Therefore, the $Co_{1.5}Mn_{1.5}O_4$/C stood out as the most effective bifunctional catalyst for both the ORR and OER among all studied $Co_{3-x}Mn_xO_4$/C catalysts, outperforming Pt/C and was even close to RuO_2/C (Figure S22). However, their stability for the OER still needs to be further improved (Figure S23).

3.3.5. OER on $Ru_{1-x-y}Mn_xCo_yO_2$/C Catalysts. Since the binary Mn and Co oxides exhibited an enhanced OER activity

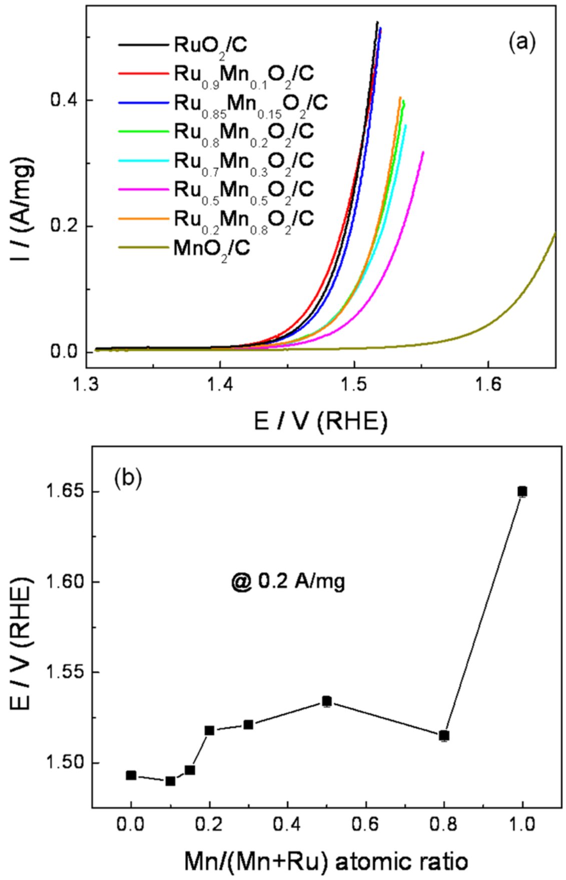

Figure 7. (a) Total metal mass-normalized LSV profiles of RuO_2/C, MnO_2/C, and $Ru_{1-x}Mn_xO_2$/C catalysts for the OER in 0.1 M KOH. Scan rate: 5 mV/s. (b) OER potential at 0.2 A/mg plotted vs Mn content. (c) ECSA-normalized LSV profiles of RuO_2/C, MnO_2/C, and $Ru_{1-x}Mn_xO_2$/C catalysts for the OER in 0.1 M KOH. (d) OER potential at 0.1 mA/cm^2 plotted vs Mn content.

when compared to pure Co and Mn oxides (Figure 8a,b), we further studied the OER on ternary Ru, Co, and Mn oxide catalysts. Total metal mass-normalized LSV profiles of the OER on $Ru_{1-x-y}Mn_xCo_yO_2$/C catalysts in 0.1 M KOH are presented in Figure 8c, and the ECSA-normalized LSV profiles are shown in Figure 8d. None of the $Ru_{1-x-y}Mn_xCo_yO_2$/C catalysts exhibited a higher OER activity than RuO_2/C in terms of both MA and SA, even after normalizing to the mass of the noble metal (Figure S24). However, the $Ru_{1-x-y}Mn_xCo_yO_2$/C catalysts were still much more active and more stable than $Co_{3-x}Mn_xO_4$/C catalysts (Figures S16f and S23).

3.3.6. OER on Ni-, Fe-, and V-Doped RuO_2/C. Other 3d transition metals such as Ni-, Fe-, and V-doped RuO_2/C catalysts were also studied for the OER in alkaline media. The total metal mass-normalized LSV profiles for the OER on $Ru_{0.9}Ni_{0.1}O_2$/C and $Ru_{0.7}Ni_{0.3}O_2$/C in 0.1 M KOH are compared with RuO_2/C in Figure 9a, and the ECSA-normalized LSV profiles are shown in Figure 9b. $Ru_{0.9}Ni_{0.1}O_2$/C and $Ru_{0.7}Ni_{0.3}O_2$/C were much less active than RuO_2/C in terms of both MA and SA. This is in contrast to the finding in acidic media.[9] Halck et al. reported that Ni-doped RuO_2 exhibited a higher OER activity than undoped RuO_2 in acidic media.[9] However, we did not observe a synergistic effect for the OER on $Ru_{0.9}Ni_{0.1}O_2$/C and $Ru_{0.7}Ni_{0.3}O_2$/C catalysts in alkaline media. Likely, Ni could be dissolved to form a rough surface with more defect sites in acidic media, which might enhance the OER.

LSV profiles of the OER on $Ru_{0.7}Fe_{0.3}O_2$/C and $Ru_{0.7}V_{0.3}O_2$/C in 0.1 M KOH are compared with RuO_2/C, $Ru_{0.7}Mn_{0.3}O_2$/C, $Ru_{0.7}Co_{0.3}O_2$/C, and $Ru_{0.7}Ni_{0.3}O_2$/C in Figure 9c,d. $Ru_{0.7}Fe_{0.3}O_2$/C and $Ru_{0.7}V_{0.3}O_2$/C catalysts did not exhibit an enhanced OER activity when compared to RuO_2/C. The OER activity of 3d transition metal-doped RuO_2/C catalysts in 0.1 M KOH decreased in the following order in terms of both MA and SA: $Ru_{0.7}Co_{0.3}O_2$/C > RuO_2/C > $Ru_{0.7}V_{0.3}O_2$/C > $Ru_{0.7}Mn_{0.3}O_2$/C > $Ru_{0.7}Ni_{0.3}O_2$/C ≈ $Ru_{0.7}Fe_{0.3}O_2$/C.

Based on data presented in Figures 2–9, the OER potentials for the most active catalysts are summarized in Table 1 for comparison. In general, Ru–TM oxide nanoparticles had 30–100 mV lower overpotentials than the respective Ru–TM alloy nanoparticles; while they also exhibited about 100 mV lower overpotential than the most active non-noble $Co_{1.5}Mn_{1.5}O_4$ nanoparticles.

3.3.7. Mn- and Co-Doped RuO_2/C as Bifunctional Catalysts for Both OER and ORR. As we reported in a previous paper, Mn- and Co-doped RuO_2/C catalysts significantly enhanced ORR activity in alkaline media when compared to pure RuO_2/C catalysts.[32] Meanwhile, Mn- and Co-doped RuO_2/C catalysts exhibited a comparable and even enhanced OER activity. Therefore, these catalysts have potential applications as effective bifunctional catalysts for both ORR and OER in alkaline media, so that a single device can function as both a fuel cell and an electrolyzer. The total overpotential (the sum of the overpotential for the ORR and

https://doi.org/10.1021/acsaem.2c01545
ACS Appl. Energy Mater. 2022, 5, 11241–11253

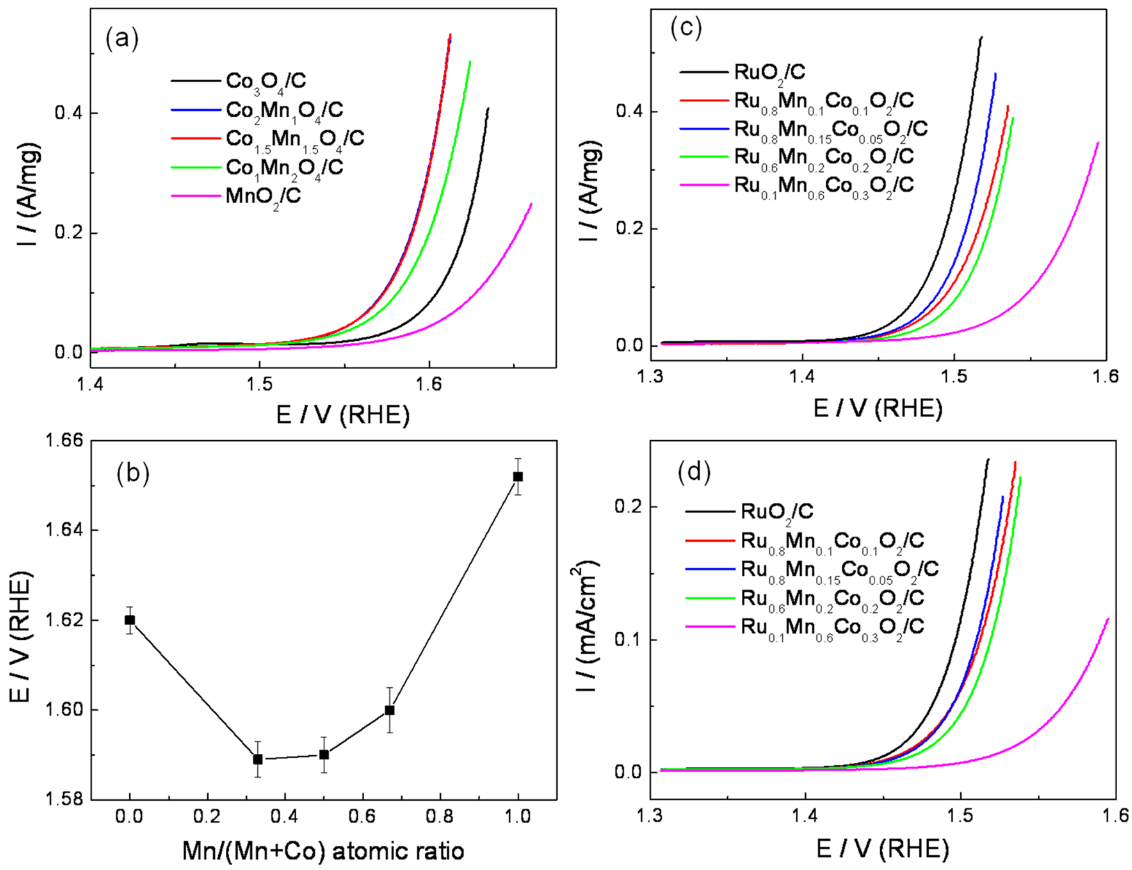

Figure 8. (a) Total metal mass-normalized LSV profiles of Co_3O_4/C, MnO_2/C, and $Co_{3-x}Mn_xO_4$/C catalysts for the OER in 0.1 M KOH. (b) OER potential at 0.2 A/mg plotted vs Mn content. (c) Total metal mass-normalized and (d) ECSA-normalized LSV profiles of RuO_2/C and $Ru_{1-x-y}Mn_xCo_yO_2$/C catalysts for the OER in 0.1 M KOH. Scan rate: 5 mV/s. The compositions are shown in the figure.

the overpotential for the OER at 2.6 mA/cm_{geo}^2) for Pt/C, RuO_2/C, $Co_{1.5}Mn_{1.5}O_4$/C, and Mn- and Co-doped RuO_2/C are compared in Figure 10. The total overpotentials for $Ru_{0.85}Mn_{0.15}O_2$/C and $Ru_{0.7}Co_{0.3}O_2$/C were 0.64 and 0.63 V, respectively, which are much smaller than 0.98 V for Pt/C, 0.84 V for $Co_{1.5}Mn_{1.5}O_4$/C, and 0.78 V for RuO_2/C. Therefore, low content Mn- and Co-doped RuO_2/C are very promising bifunctional catalysts for both ORR and OER in alkaline fuel cells/electrolyzers.

4. DISCUSSION

The OER involves the formation of adsorbed O atoms and their combination to form O_2. A volcano-shaped curve for the OER activity vs the formation energy of the metal oxides was reported by Trasatti several decades ago.[1,5] Among them, RuO_2 exhibited the highest OER in both acidic and alkaline media, and IrO_2 was the second most active metal oxide. Among the individual non-noble metal oxides, Co_3O_4 and MnO_2 also exhibited high OER activity in alkaline media. $Co_{3-x}Mn_xO_4$ nanoparticles exhibited a synergistic enhancement for the OER when compared to Co_3O_4 and MnO_2 nanoparticles. The synergistic enhancement was also observed for the ORR on $Co_{3-x}Mn_xO_4$ nanoparticles.[32] Therefore, $Co_{1.5}Mn_{1.5}O_4$ nanoparticles can be used as the most effective non-noble-metal bifunctional catalysts for both ORR and OER in alkaline media. However, they are still much less active than Co- or Mn-doped RuO_2 nanoparticles. Co-doped RuO_2 nanoparticles exhibited higher OER activity than RuO_2 in alkaline media, similar to the case in acidic media as reported in ref 9. Ni-doped RuO_2 was also reported to be more active than RuO_2 in acidic media.[9] However, in alkaline media, we did not observe an enhancement of the OER activity for Ni-doped RuO_2 nanoparticles. This might be due to different electrolytes with very different pH values, which could change the surface chemistry of catalysts and even the reaction mechanism,[45−47] and/or increased surface area caused by Ni dissolution in acidic media.

IrO_2/C and $Ru_{1-x}Ir_xO_2$/C were not successfully synthesized since they require higher annealing temperatures in air when $IrCl_3$ is used as a precursor. However, when carbon black was used as the catalyst support, high annealing temperatures could burn the carbon black causing a loss of support. Metal oxide supports could be an attractive alternative to carbon black for preparing supported IrO_2-based catalysts.

As mentioned before, the Ir/C nanoparticle catalyst is more active than the bulk Ir electrode for the OER in alkaline media in terms of SA. In contrast, it was reported that in acidic media, bulk Ir was slightly more active than Ir/C.[7] Pt/C and Ru/C exhibited significantly lower OER activity than the corresponding bulk electrodes in alkaline media. This is similar to the activity trends in acid media.[7] Therefore, when extending the OER activity from bulk electrodes to nanoparticles, the nanoparticle size effect on the OER activity must be considered. For the hydrogen oxidation/evolution reactions in alkaline media, we also found that the Rh/C nanoparticle catalysts were much superior to bulk Rh electrodes in terms of SA, while Pt/C and Ir/C were less active than the respective Pt and Ir bulk electrodes.[41]

https://doi.org/10.1021/acsaem.2c01545
ACS Appl. Energy Mater. 2022, 5, 11241−11253

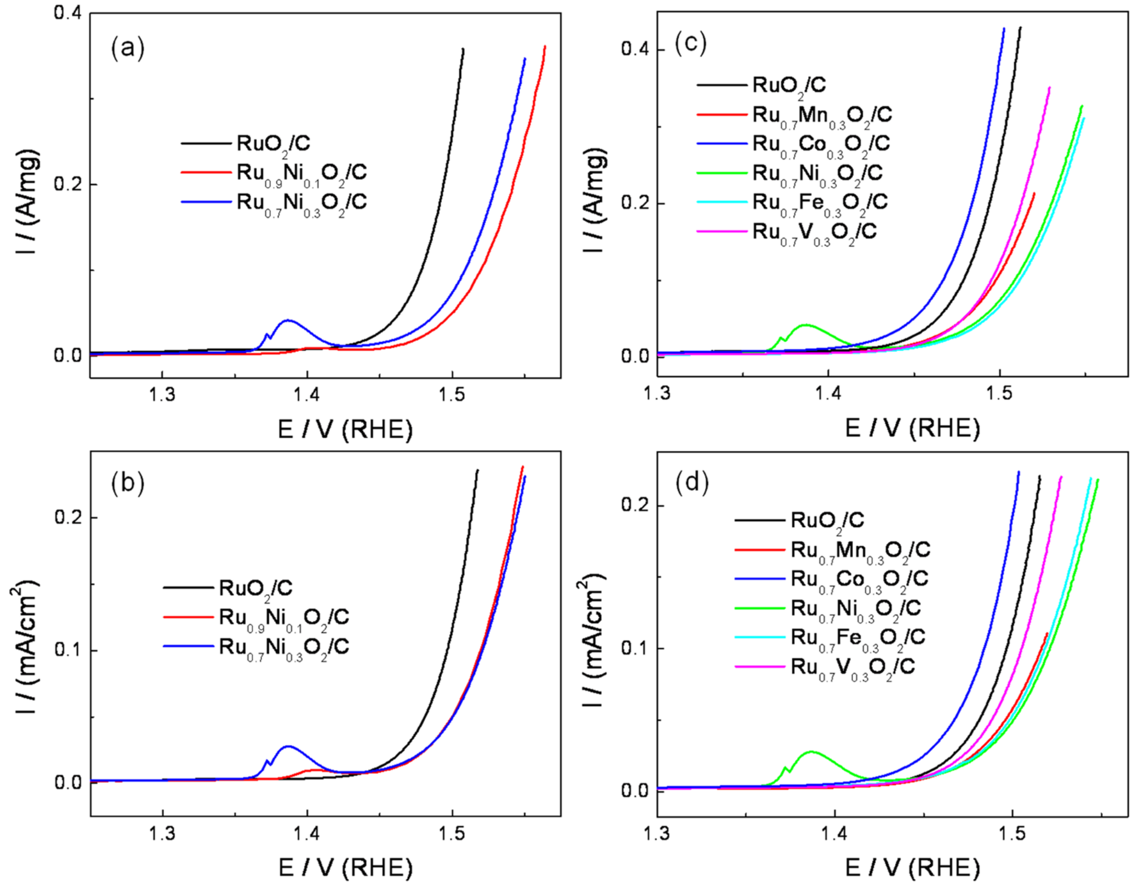

Figure 9. (a) Total metal mass-normalized and (b) ECSA-normalized LSV profiles of RuO_2/C, $Ru_{0.9}Ni_{0.1}O_2/C$, and $Ru_{0.7}Ni_{0.3}O_2/C$ catalysts for the OER in 0.1 M KOH. (c) Total metal mass-normalized and (d) ECSA-normalized LSV profiles of RuO_2/C, $Ru_{0.7}Co_{0.3}O_2/C$, $Ru_{0.7}Mn_{0.3}O_2/C$, $Ru_{0.7}Ni_{0.3}O_2/C$, $Ru_{0.7}Fe_{0.3}O_2/C$, and $Ru_{0.7}V_{0.3}O_2/C$ catalysts for the OER in 0.1 M KOH. Scan rate: 5 mV/s. The compositions are shown in the figure.

Table 1. Summary of OER Potentials (E) of Most Active Carbon-Supported Ru−M Alloy (M = Ir, Co, Ni, or Fe), Ru−TM Oxide (TM = Co, Mn, Ni, Fe, or V), and $Co_{1.5}Mn_{1.5}O_4$ Nanoparticles, Compared to Pure Ru and Ir Bulk and Nanoparticle Catalysts[a]

metal catalysts	E_{MA} (V)	E_{SA} (V)	$E_{MA\text{-}nm}$ (V)	metal oxide catalysts	E_{MA} (V)	E_{SA} (V)	$E_{MA\text{-}nm}$ (V)
bulk Ir	NA	1.530	NA	RuO_2/C	1.493	1.497	1.493
Ir/C	1.526	1.507	1.526	$Ru_{0.7}Co_{0.3}O_2/C$	1.483	1.484	1.478
Bulk Ru	NA	1.350	NA	$Ru_{0.5}Co_{0.5}O_2/C$	1.483	1.485	1.472
Ru/C	>1.8	>1.8	>1.8	$Ru_{0.9}Mn_{0.1}O_2/C$	1.490	1.494	1.487
$Ru_{0.7}Ir_{0.3}/C$	1.526	1.512	1.526	$Ru_{0.85}Mn_{0.15}O_2/C$	1.496	1.500	1.493
$Ru_{0.3}$ $Ir_{0.7}/C$	1.528	1.511	1.528	$Ru_{0.2}Mn_{0.8}O_2/C$	1.515	1.531	1.489
$Ru_{0.7}Co_{0.3}/C$	1.552	1.558	1.527	$Co_{1.5}Mn_{1.5}O_4/C$	1.589	1.600	NA
$Ru_{0.5}Co_{0.5}/C$	1.573	1.595	1.555	$Ru_{0.8}Mn_{0.15}Co_{0.05}O_2/C$	1.507	1.510	1.505
$Ru_{0.7}Ni_{0.3}/C$	1.586	1.581	1.577	$Ru_{0.7}Ni_{0.3}O_2/C$	1.530	1.521	1.523
$Ru_{0.7}Fe_{0.3}/C$	1.662	1.656	1.658	$Ru_{0.7}Fe_{0.3}O_2/C$	1.533	1.518	1.526
$Ru_{0.5}Fe_{0.5}/C$	1.657	1.649	1.645	$Ru_{0.7}V_{0.3}O_2/C$	1.513	1.505	1.503

[a]E_{MA} and E_{SA} denote the OER potentials at 0.2 A/mg and 0.1 mA/cm^2, respectively. $E_{MA\text{-}nm}$ represents the OER potential at 0.2 A/mg$_{nm}$. Error bars are shown in Figures 2−9.

Ru−TM/C (TM = Co, Ni, and Fe) alloy nanoparticles exhibited higher OER activity than Ru/C. Moreover, all studied Ru−TM oxide nanoparticles were more active than their respective Ru−TM alloy nanoparticles for the OER in alkaline media. This might be due to the relatively weaker oxygen adsorption on oxides than on alloys.[31,32] Oxygen adsorption energies on Ru(0001) were calculated with density functional theory (DFT) to be −1.5446 eV at atop sites (smallest) and −3.1395 eV at hcp sites (largest), respectively (Table S3). In contrast, the oxygen adsorption energy on $RuO_2(110)$ is only −0.7413 eV.[31,32] In the previous paper,[32] a volcano-shaped relationship between the ORR activity of $Ru_{1-x}TM_xO_2/C$ (TM = Co, Mn, Ni, Fe, and V) and O adsorption energy was observed in alkaline media. Co- and Mn-doped RuO_2/C catalysts were found to be the most active for the ORR due to the modest O adsorption energies. O adsorption on Ni- and Fe-doped RuO_2 was too weak, so that O_2 was hardly dissociated, and thus a low ORR activity was

https://doi.org/10.1021/acsaem.2c01545
ACS Appl. Energy Mater. 2022, 5, 11241−11253

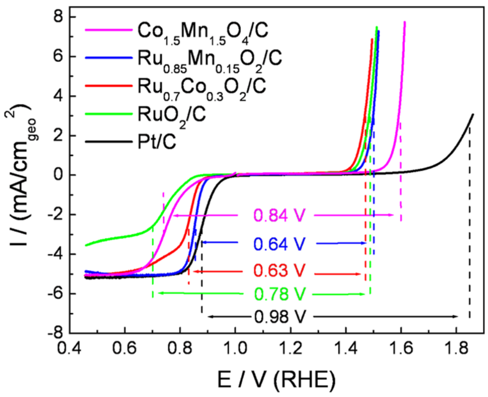

Figure 10. Comparison of the overpotential for both ORR and OER on $Co_{1.5}Mn_{1.5}O_4/C$, $Ru_{0.85}Mn_{0.15}O_2/C$, $Ru_{0.7}Co_{0.3}O_2/C$, RuO_2/C, and Pt/C at 2.6 mA/cm_{geo}^2. Scan rate: 5 mV/s. Rotation rate: 1600 rpm. The catalyst loading was 14 $\mu g_{metal}/cm_{geo}^2$.

observed. In contrast, O adsorption on RuO_2 and V-doped RuO_2 was too strong, so that adsorbed O was difficult to desorb, thus leading to a low ORR activity.[32] However, RuO_2 exhibited quite high activity for the OER in alkaline media. This might be caused by the further oxidation of RuO_2 surfaces to higher Ru valence states,[43] on which O adsorption becomes weaker. For Co-doped RuO_2, the oxygen adsorption at Co and Ru sites was even weaker than on Co_3O_4 and RuO_2, respectively (Table S3), and thus the $Ru_{1-x}Co_xO_2$ (x = 0.3–0.5) exhibited even higher OER activity than Co_3O_4 and RuO_2. Regarding Mn-doped RuO_2, the O adsorption energy at Ru sites increased relative to that for RuO_2, while the O adsorption at Mn became weaker than that for MnO_2 (Table S3), so that Mn-doped RuO_2 did not enhance the OER kinetics significantly when compared to RuO_2. The O adsorption at octahedral Co sites of $Co_{3-x}Mn_xO_4$ was weaker than that on Co_3O_4 (Table S3), and thus $Co_{3-x}Mn_xO_4$ exhibited higher OER activity than Co_3O_4/C. We believe that the OER takes place at octahedral Co sites, while Mn provides electronic effects to lower the adsorption energy of oxygen.

5. CONCLUSIONS

We have synthesized a series of carbon-supported Ru−M (M = Co, Ni, Fe, or Ir) alloy nanoparticle catalysts and a series of carbon-supported 3d transition metals (TMs = Co, Ni, Fe, Mn, or V)-doped RuO_2 nanoparticle catalysts *via* a wet-impregnation method, followed by annealing in forming gas and in air, respectively. For comparison, other carbon-supported catalysts—Pt/C, Ir/C, RuO_2/C, MnO_2/C, Co_3O_4/C, and $Co_{3-x}Mn_xO_4$/C nanoparticles—were also synthesized. These catalysts were characterized by XRD, EDX, XPS, TEM, TGA, and RDE voltammetry. All synthesized Ru−M alloy nanoparticles and Ru−TM oxide nanoparticles had a small mean nanoparticle size of 3−7 nm. Their intrinsic OER activity in alkaline media was compared.

We found that Ir/C was the most active among pure metal nanoparticle catalysts for the OER in alkaline media and was even superior to a bulk Ir electrode. Although a bulk Ru electrode was very active for the OER, it dissolved very fast during the OER. In contrast, Ru/C exhibited very low OER activity. Alloying Ru nanoparticles with Ir, Co, Ni, or Fe enhanced their OER activity. $Ru_{1-x}Ir_x$/C ($x \geq 0.3$) exhibited the highest OER activity among all Ru alloy nanoparticle catalysts and had comparable OER activity to Ir/C. $Ru_{0.7}Co_{0.3}$/C was the most active among all studied Ru−Co alloy nanoparticle catalysts and even outperformed Ir/C at low overpotentials. $Ru_{0.7}Ni_{0.3}$/C was inferior to $Ru_{0.7}Co_{0.3}$/C, but more active than $Ru_{0.7}Fe_{0.3}$/C.

In general, the TM-doped RuO_2/C nanoparticle catalysts exhibited higher OER activity than the respective Ru−TM/C alloy nanoparticle catalysts. Small amounts of Mn (≤0.15) doped into RuO_2/C yielded slightly enhanced or comparable OER activity to RuO_2/C. Further increases in the Mn content caused the loss of OER activity. Small amounts of Co-doped RuO_2/C catalysts also exhibited comparable OER activity to RuO_2/C. In contrast, 30−50 atom % of Co-doped RuO_2/C significantly enhanced the OER in alkaline media and were the most active among all studied catalysts. Ni-, Fe-, and V-doped RuO_2/C did not promote OER kinetics when compared to RuO_2/C.

Moreover, $Ru_{1-x}Mn_xO_2$/C ($x \approx 0.15$) and $Ru_{1-x}Co_xO_2$/C (x = 0.3−0.5) nanoparticles were found to be the most effective bifunctional catalysts for both the ORR and OER in alkaline media. $Co_{3-x}Mn_xO_4$/C ($x \approx 1.5$) nanoparticles can also be used as very effective nonprecious-metal-based bifunctional catalysts for both the ORR and OER in alkaline media and are even more efficient than Pt/C. However, they are still less active than $Ru_{1-x}Mn_xO_2$/C ($x \approx 0.15$) and $Ru_{1-x}Co_xO_2$/C (x = 0.3−0.5) nanoparticles.

■ ASSOCIATED CONTENT

Supporting Information

The Supporting Information is available free of charge at https://pubs.acs.org/doi/10.1021/acsaem.2c01545.

Table of physical properties, XRD data, TEM images, EDX spectra, XPS spectra, and TGA data of carbon-supported Ru−TM alloy and TM-doped RuO_2 nanoparticle catalysts as well as Pt/C, Ir/C, Ru/C, RuO_2/C, MnO_2/C, Co_3O_4/C, and $Co_{3-x}Mn_xO_4$/C; cyclic voltammograms of these catalysts; RDE voltammograms and Tafel plots for the OER on these catalysts in 0.1 M KOH; and oxygen adsorption energies calculated with DFT (PDF)

■ AUTHOR INFORMATION

Corresponding Author

Héctor D. Abruña − *Department of Chemistry and Chemical Biology, Baker Laboratory, Cornell University, Ithaca, New York 14853-1301, United States;* orcid.org/0000-0002-3948-356X; Email: hda1@cornell.edu

Author

Hongsen Wang − *Department of Chemistry and Chemical Biology, Baker Laboratory, Cornell University, Ithaca, New York 14853-1301, United States;* orcid.org/0000-0001-7926-2895

Complete contact information is available at: https://pubs.acs.org/10.1021/acsaem.2c01545

Notes

The authors declare no competing financial interest.

■ ACKNOWLEDGMENTS

This work was supported as part of the Center for Alkaline Based Energy Solutions (CABES) at Cornell, an Energy

Frontier Research Center funded by the U.S. Department of Energy, Office of Science, Office of Basic Energy Sciences under Award Number DE-SC0019445. This work made use of the Cornell Center for Materials Research Facilities supported by the National Science Foundation under Award Number DMR-1719875.

REFERENCES

(1) Trasatti, S. Electrocatalysis by Oxides - Attempt at a Unifying Approach. *J. Electroanal. Chem. Interfacial Electrochem.* **1980**, *111*, 125−131.

(2) Lee, Y.; Suntivich, J.; May, K. J.; Perry, E. E.; Shao-Horn, Y. Synthesis and Activities of Rutile IrO_2 and RuO_2 Nanoparticles for Oxygen Evolution in Acid and Alkaline Solutions. *J. Phys. Chem. Lett.* **2012**, *3*, 399−404.

(3) Cherevko, S.; Geiger, S.; Kasian, O.; Kulyk, N.; Grote, J.-P.; Savan, A.; Shrestha, B. R.; Merzlikin, S.; Breitbach, B.; Ludwig, A.; Mayrhofer, K. J. J. Oxygen and Hydrogen Evolution Reactions on Ru, RuO_2, Ir, and IrO_2 Thin Film Electrodes in Acidic and Alkaline Electrolytes: A Comparative Study on Activity and Stability. *Catal. Today* **2016**, *262*, 170−180.

(4) Kötz, R.; Stucki, S. Oxygen Evolution and Corrosion on Ruthenium-Iridinm Alloys. *J. Electrochem. Soc.* **1985**, *132*, 103−107.

(5) Trasatti, S. Electrocatalysis in the Anodic Evolution of Oxygen and Chlorine. *Electrochim. Acta* **1984**, *29*, 1503−1512.

(6) Antolini, E. Iridium as Catalyst and Cocatalyst for Oxygen Evolution/Reduction in Acidic Polymer Electrolyte Membrane Electrolysers and Fuel Cells. *ACS Catal.* **2014**, *4*, 1426−1440.

(7) Reier, T.; Oezaslan, M.; Stasser, P. Electrocatalytic Oxygen Evolution Reaction (OER) on Ru, Ir, and Pt Catalysts: A Comparative Study of Nanoparticles and Bulk Materials. *ACS Catal.* **2012**, *2*, 1765−1772.

(8) Danilovic, N.; Subbaraman, R.; Chang, K.-C.; Chang, S. H.; Kang, Y. J.; Snyder, J.; Paulikas, A. P.; Strmcnik, D.; Kim, Y.-T.; Myers, D.; Stamenkovic, V. R.; Markovic, N. M. Activity-Stability Trends for the Oxygen Evolution Reaction on Monometallic Oxides in Acidic Environments. *J. Phys. Chem. Lett.* **2014**, *5*, 2474−2478.

(9) Halck, N. B.; Petrykin, V.; Krtil, P.; Rossmeisl, J. Beyond the Volcano Limitations in Electrocatalysis - Oxygen Evolution Reaction. *Phys. Chem. Chem. Phys.* **2014**, *16*, 13682−13688.

(10) Forgie, R.; Bugosh, G.; Neyerlin, K. C.; Liu, Z.; Strasser, P. Bimetallic Ru Electrocatalysts for the OER and Electrolytic Water Splitting in Acidic Media. *Electrochem. Solid-State Lett.* **2010**, *13*, B36−B39.

(11) Huang, Z.-F.; Wang, J.; Peng, Y.; Jung, C.-Y.; Fisher, A.; Wang, X. Design of Efficient Bifunctional Oxygen Reduction/Evolution Electrocatalyst: Recent Advances and Perspectives. *Adv. Energy Mater.* **2017**, *7*, No. 1700544.

(12) Browne, M. P.; Nolan, H.; Duesberg, G. S.; Colavita, P. E.; Lyons, M. E. G. Low-Overpotential High-Activity Mixed Manganese and Ruthenium Oxide Electrocatalysts for Oxgen Evolution Reaction in Alkaline Media. *ACS Catal.* **2016**, *6*, 2408−2415.

(13) Hutchings, R.; Müller, K.; Kötz, R.; Stucki, S. A Structural Investigation of Stabilized Oxygen Evolution Catalysts. *J. Mater. Sci.* **1984**, *19*, 3987−3994.

(14) Yeo, R. S.; Orehotsky, J.; Visscher, W.; Srinivasan, S. Ruthenium-Based Mixed Oxides as Electrocatalysts for Oxygen Evolution in Acid Electroltes. *J. Electrochem. Soc.* **1981**, *128*, 1900−1904.

(15) Kim, J.; Shih, P.-C.; Tsao, K.-C.; Pan, Y.-T.; Yin, X.; Sun, C.-J.; Yang, H. High-Performance Pyrochlore-Type Yttrium Ruthenate Electrocatalyst for Oxygen Evolution Reaction in Acidic Media. *J. Am. Chem. Soc.* **2017**, *139*, 12076−12083.

(16) Liang, Y.; Li, Y.; Wang, H.; Zhou, J.; Wang, J.; Regier, T.; Dai, H. Co_3O_4 Nanocrystals on Graphene as a Synergistic Catalyst for Oxygen Reduction Reaction. *Nat. Mater.* **2011**, *10*, 780−786.

(17) Liang, Y.; Wang, H.; Zhou, J.; Li, Y.; Wang, J.; Regier, T.; Dai, H. Covalent Hybrid of Spinel Mangnese-Cobalt Oxide and Graphene as Advanced Oxygen Reduction Electrocatalysts. *J. Am. Chem. Soc.* **2012**, *134*, 3517−3523.

(18) Burke, M. S.; Zou, S.; Enman, L. J.; Kellon, J. E.; Gabor, C. A.; Pledger, E.; Boettcher, S. W. Revised Oxygen Evolution Reaction Activity Trends for First-Row Transition-Metal (Oxy)hydroxides in Alkaline Media. *J. Phys. Chem. Lett.* **2015**, *6*, 3737−3742.

(19) Yeo, B. S.; Bell, A. T. Enhanced Activity of Gold-Supported Cobalt Oxide for the Electrochemical Evolution of Oxygen. *J. Am. Chem. Soc.* **2011**, *133*, 5587−5593.

(20) Fabbri, E.; Habereder, A.; Waltar, K.; Kötz, R.; Schmidt, T. J. Developments and Perspectives of Oxide-Based Catalysts for the Oxygen Evolution Reaction. *Catal. Sci. Technol.* **2014**, *4*, 3800−3821.

(21) Osgood, H.; Devaguptapu, S. V.; Xu, H.; Cho, J.; Wu, G. Transition Metal (Fe, Co, Ni, and Mn) oxides for Oxygen Reduction and Evolution Bifunctional Catalysts in Alkaline Media. *Nano Today* **2016**, *11*, 601−625.

(22) Stevens, M. B.; Trang, C. D. M.; Enman, L. J.; Deng, J.; Boettcher, S. W. Reactive Fe-Sites in Ni/Fe (Oxy)hydroxide Are Responsible for Exceptional Oxygen Electrocatalysis Activity. *J. Am. Chem. Soc.* **2017**, *139*, 11361−11364.

(23) Luo, J.; Im, J.-H.; Mayer, M. T.; Schreier, M.; Nazeeruddin, M. K.; Park, N.-G.; Tilley, S. D.; Fan, H. J.; Grätzel, M. Water Photolysis at 12.3% Efficiency via Perovskite Photovoltaics and Earth-Abundant Catalysts. *Science* **2014**, *345*, 1593−1596.

(24) Dionigi, F.; Strasser, P. NiFe-Based (Oxy)hydroxide Catalysts for Oxygen Evolution Reaction in Non-Acidic Electrolytes. *Adv. Energy Mater.* **2016**, *6*, No. 1600621.

(25) Li, X.; Walsh, F. C.; Pletcher, D. Nickel Based Electrocatalysts for Oxygen Evolution in High Current Density, Alkaline Water Electrolysers. *Phys. Chem. Chem. Phys.* **2011**, *13*, 1162−1167.

(26) Corrigan, D. A. The Catalysis of the Oxygen Evolution Reaction by Iron Impurities in Thin Film Nickel Oxide Electrodes. *J. Electrochem. Soc.* **1987**, *134*, 377−384.

(27) Miller, E. L.; Rocheleau, R. E. Electrochemical Behavior of Reactively Sputtered Iron-Doped Nickel Oxide. *J. Electrochem. Soc.* **1997**, *144*, 3072−3077.

(28) Gong, M.; Li, Y.; Wang, H.; Liang, Y.; Wu, J. Z.; Zhou, J.; Wang, J.; Regier, T.; Wei, F.; Dai, H. An Advanced Ni-Fe Layered Double Hydroxide Electrocatalyst for Water Oxidation. *J. Am. Chem. Soc.* **2013**, *135*, 8452−8455.

(29) Man, I. C.; Su, H.-Y.; Calle-Vallejo, F.; Hansen, H. A.; Martinez, J. I.; Inoglu, N. G.; Kitchin, J.; Jaramillo, T. F.; Nørskov, J. K.; Rossmeisl, J. Universality in Oxygen Evolution Electrocatalysis on Oxide Surfaces. *ChemCatChem* **2011**, *3*, 1159−1165.

(30) Suntivich, J.; May, K. J.; Gasteiger, H. A.; Goodenough, J. B.; Shao-Horn, Y. A Perovskite Oxide Optimized for Oxygen Evolution Catalysis from Molecular Orbital Principles. *Science* **2011**, *334*, 1383−1385.

(31) Wang, H.; Yang, Y.; DiSalvo, F. J.; Abruña, H. D. Multifunctional Electrocatalysts: Ru-M (M = Co, Ni, Fe) for Alkaline Fuel Cells and Electrolyzers. *ACS Catal.* **2020**, *10*, 4608−4616.

(32) Wang, H.; Abruña, H. D. Single-Phase $Ru_{1-x-y}Mn_xCo_yO_2$ Nanoparticles as Highly Effective Oxygen Reduction Electrocatalysts in Alkaline Media with Enhanced Stability and Fuel-Tolerance. *Appl. Catal., B* **2020**, *277*, No. 119149.

(33) Shao, M.; Peles, A.; Shoemaker, K. Electrocatalysis on Platinum Nanoparticles: Particle Size Effect on Oxygen Reduction Reaction Activity. *Nano Lett.* **2011**, *11*, 3714−3719.

(34) Arenz, M.; Mayrhofer, K. J. J.; Stamenkovic, V.; Blizanac, B. B.; Tomoyuki, T.; Ross, P. N.; Markovic, N. M. The Effect of the Particle Size on the Kinetics of CO Electrooxidation on High Surface Area Pt Catalysts. *J. Am. Chem. Soc.* **2005**, *127*, 6819−6829.

(35) Bergamaski, K.; Pinheiro, A. L. N.; Teixeira-Neto, E.; Nart, F. C. Nanoparticle Size Effects on Methanol Electrochemical Oxidation on Carbon Supported Platinum Catalysts. *J. Phys. Chem. B* **2006**, *110*, 19271−19279.

(36) Zheng, J.; Zhou, S.; Gu, S.; Xu, B.; Yan, Y. Size-Dependent Hydrogen Oxidation and Evolution Activities on Supported

Palladium Nanoparticles in Acid and Base. *J. Electrochem. Soc.* **2016**, *163*, F499−F506.
(37) Zhou, W.; Lee, J. Y. Particle Size Effects in Pd-Catalyzed Electrooxidation of Formic Acid. *J. Phys. Chem. C* **2008**, *112*, 3789−3793.
(38) Takasu, Y.; Iwazaki, T.; Sugimoto, W.; Murakami, Y. Size Effects of Platinum Particles on the Electro-oxidation of Methanol in an Aqueous Solution of $HClO_4$. *Electrochem. Commun.* **2000**, *2*, 671−674.
(39) Yang, F.; Zhang, Q.; Liu, Y.; Chen, S. A Theoretical Consideration on the Surface Structure and Nanoparticle Size Effects of Pt in Hydrogen Electrocatalysis. *J. Phys. Chem. C* **2011**, *115*, 19311−19319.
(40) Velasco-Vélez, J.-J.; Carbonio, E. A.; Chuang, C.-H.; Hsu, C.-J.; Lee, J.-F.; Arrigo, R.; Hävecker, M.; Wang, R.; Plodinec, M.; Wang, F. R.; Centeno, A.; Zurutuza, A.; Falling, L. J.; Mom, R. V.; Hofmann, S.; Schlögl, R.; Knop-Gericke, A.; Jones, T. E. Surface Electron-Hole Rich Species Active in the Electrocatalytic Water Oxidation. *J. Am. Chem. Soc.* **2021**, *143*, 12524−12534.
(41) Wang, H.; Abruña, H. D. Rh and Rh Alloy Nanoparticles as Highly Active H_2 Oxidation Catalysts for Alkaline Fuel Cells. *ACS Catal.* **2019**, *9*, 5057−5062.
(42) Burke, L. D.; Whelan, D. P. The Behaviour of Ruthenium Anode in Base. *J. Electroanal. Chem. Interfacial Electrochem.* **1979**, *103*, 179−187.
(43) Povar, I.; Spinu, O. Ruthenium Redox Equilibria: 3. Pourbaix Diagrams for the Systems Ru-H_2O and Ru-Cl^--H_2O. *J. Electrochem. Sci. Eng.* **2016**, *6*, 145−153.
(44) Medway, S. L.; Lucas, C. A.; Kowal, A.; Nichols, R. J.; Johnson, D. In situ Studies of the Oxidation of Nickel Electrodes in Alkaline Solution. *J. Electroanal. Chem.* **2006**, *587*, 172−181.
(45) Ramaswamy, N.; Mukerjee, S. Influence of Inner- and Outer-Sphere Electron Transfer Mechanisms during Electrocatalysis of Oxygen Reduction in Alkaline Media. *J. Phys. Chem. C* **2011**, *115*, 18015−18026.
(46) Rojas-Carbonell, S.; Artyushkova, K.; Serov, A.; Santoro, C.; Matanovic, I.; Atanassov, P. Effect of pH on the Activity of Platinum Group Metal-Free Catalysts in Oxygen Reduction Reaction. *ACS Catal.* **2018**, *8*, 3041−3053.
(47) Liang, Q.; Brocks, G.; Bieberle-Hütter, A. Oxygen Evolution Reaction (OER) Mechanism under Alkaline and Acidic Conditions. *J. Phys. Energy* **2021**, *3*, No. 026001.

https://doi.org/10.1021/acsaem.2c01545
ACS Appl. Energy Mater. 2022, 5, 11241−11253